Dynamical and thermodynamical features in the fragmentation process

J.P. Wieleczko[a], R. Bougault[b], A. Chbihi[a], D. Durand[b], C. Escano Rodriguez[a], and J.D. Frankland[a]
[a]*GANIL, CEA et IN2P3-CNRS, B.P. 5027, F-14076 Caen Cedex, France.*
[b]*LPC, IN2P3-CNRS, ENSI-Caen et Université, F-14050 Caen Cedex, France.*

Recibido el 28 de febrero de 2006; aceptado el 18 de junio de 2006

Dynamical and thermodynamical features of the fragmentation process around the Fermi energy are discussed using data measured at GANIL and GSI facilities with the 4π array INDRA. Presented topics address transport properties and transition phenomena in central and peripheral collisions and give a panorama on the physics of transient systems produced in heavy-ion collisions.

Keywords: Nuclear stopping; scaling laws; fluctuations; heat capacity; fragmentation.

Se discuten propiedades dinámicas y termodinámicas del proceso de fragmentación cerca de la energía de Fermi con datos experimentales obtenidos en GANIL y GSI con el arreglo 4π INDRA. Se estudian las propiedades de transporte y fenómenos transitorios in colisiones centrales y periféricas y se presenta un panorama de la física de sistemas transitorios producidos en colisiones de iones pesados.

Descriptores: Frenamiento nuclear; leyes de escala; fluctuaciones; capacidad calorífica; fragmentación.

PACS: 25.70.-z; 25.70.Lm; 25.70.Pq

1. Introduction

The study of the nuclear matter from nuclei to stars is one of the major goals of the modern physics. Nucleus-Nucleus collisions are the adequate tool for such a study as they offer large panoply of initial conditions that allow varying external parameters relevant to measure properties of nuclear matter under extreme conditions. Since nuclear forces resemble to a Van der Waals interaction the nuclear matter is expected to present a liquid-gas phase transition. In central collisions at incident energies around the Fermi energy, a compression-expansion cycle could be triggered, driving the system towards a part of the phase diagram where mechanical instabilities could set in, leading to an abundant production of fragments. Indeed, since a long time the fragmentation process has been mostly interpreted as a signature of a liquid-gas phase transition. However, fragmentation is observed in nuclear reactions over a wide incident energy range, and in various centrality conditions, suggesting different explorations across the phase diagram. The present contribution gives a flavour of these aspects that characterise the nuclear fragmentation at intermediate energy.

2. The 4π INDRA array

The 4π INDRA array is described in detail in Ref. 1, and the main specifications are listed here. INDRA is made of 336 cells arranged in 17 rings; the first one (2-3°) is an array of plastic scintillators. Rings 2 to 9 (polar angle from 3 to 45°) consist in three layers comprising an ionisation chamber (IoCh) followed by a solid state silicon detector (Si) and a Cesium Iodide scintillator (CsI(Tl)). The angular range (45 to 176°) is covered with two layers detector IoCh/CsI. The device provides 90% of 4π geometrical efficiency, a charge identification from H to U, and a mass resolution up to Beryllium.

3. Nuclear stopping

Nuclear stopping in central heavy-ion collisions at intermediate energies is of crucial importance as it characterises the properties of the transient system produced during the reaction, and improves the constraints on the basic ingredients of the microscopic transport models. A wide and systematic body of data has been collected for various entrance channels with total sizes between 80 and 400 mass units on a range of bombarding energy crossing the Fermi energy (see for example [2]. In the present contribution, the nuclear stopping is deduced from the degree of anisotropy in momentum space using components along and transverse to the incoming momentum direction $R_{iso} = \sum E_{per}/2\sum E_{par}$ where E_{per} (E_{par}) is the centre of mass (c.o.m) transverse (parallel) energy. Events are selected using two criteria:

i) only charged particles emitted in the forward hemisphere are considered;

ii) events are kept if the total collected charge of the forward hemisphere in the c.o.m is larger than 90% of the projectile charge.

Then, R_{iso} is calculated for the total multiplicity of charged products. A saturation of R_{iso} value is observed for the highest multiplicities. We then calculate the average value of R_{iso} weighted by the multiplicity distribution in the saturation domain. The final value is called $\langle R_{cent}\rangle$. The data set corresponds to 1% of the measured events.

The upper panel of Fig. 1 (extracted from [3]) shows the bombarding energy and size systems dependence of $\langle R_{cent}\rangle$. Let us start with the Xe+Sn reaction measured from 25 A MeV up to 100 A MeV. All values are below unity showing that a full equilibration is not reached in the explored energy range. $\langle R_{cent}\rangle$ decreases as the beam energy increases and starts to increases above 40 A MeV. Ni+Ni reactions show similar trends but the minimum is reached

around 50 A MeV. For Au+Au reactions a linear behaviour is observed above 40 A MeV and further investigations at lower bombarding energy are needed. For the lighter system, Ar+KCl one observes a continuous decreasing of $\langle R_{cent} \rangle$ and the linear regime at high bombarding energy is not seen and could start above 70 A MeV. Even though our data set covers a large variety of reaction, it is evident that investigations are needed for light systems at high energies and for heavier systems at low energies. However, from the data set it is possible to extract an energy of transition increasing as the total size decreases. The first idea is to propose a transition between two regimes: the first one is the mean field regime at low beam energies; the second one is the nucleon-nucleon regime at high bombarding energies. To go further in that direction the $\langle R_{cent} \rangle$ values have been scaled by the radius of half of the total system. The results are shown on the lower part in Fig. 1. All data are roughly scaled at high energy, which corroborates the idea of a regime dominated by nucleon-nucleon collisions. The interesting feature is the energy and the size dependence of the transition energy that could be used as constraints to study the in-medium effects in microscopic transport models. It is worth noticing that using a different centrality selector, the authors of [4] have shown that part of the central events could be explained within a statistical approach assuming a prolate shape with a main axis pointing along the beam direction. This could be a mimic of the stopping power measured using $\langle R_{cent} \rangle$ and indicates that dynamical and thermodynamical features are strongly intricate.

Such a situation is likely in nuclear collisions at intermediate energies. This is the reason why model independent procedures are very demanding. The theory of the universal order parameter fluctuations in finite systems has been proposed to address the question of phase transition in heavy-ion

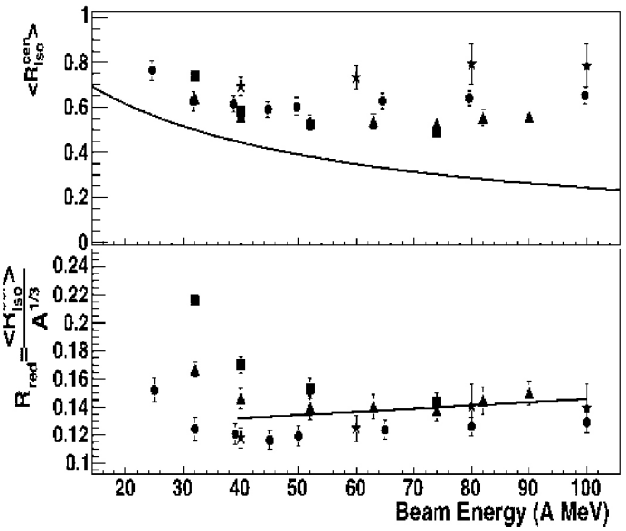

FIGURE 1. Top: evolution of $\langle R_{cent} \rangle$ as a function of the beam energy for central collisions and various systems: (stars) Au+Au, (dot) Xe+Sn, (triangles) Ni+Ni, (squares) Ar+KCl. Bottom: same reactions as above for the scaled isotropy ratio $\langle R_{cent} \rangle / A^{1/3}$.

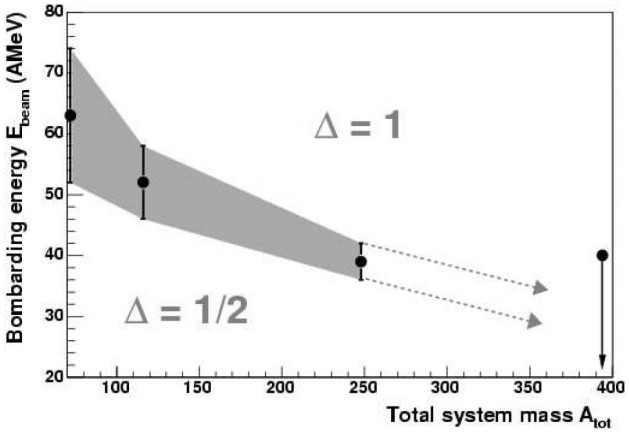

FIGURE 2. Dependence on incident energy and total system mass of the frontier between the two Δ-scaling regimes for very central collisions [6].

collisions [5]. This theory has been applied on the set of data used to study the nuclear stopping [6]. Evidence has been found that the largest fragment in each event plays the role of an order parameter. According to the scaling properties of its fluctuations (so called Δ-scaling) the largest fragment delineates two regimes at low and high bombarding energy. In each regime, the distribution of the largest fragment collapses to an approximately universal scaling function with Δ=0.5 (Δ=1.) at low (high) bombarding energy. The dependence on incident energy and total mass of the system of the transition between the two regimes are shown in Fig. 2. What is worth noticing is the similarity between the energy at which the stopping power indicates the transition from a mean field regime to a nucleon-nucleon regime in one side, and the transition from an ordered phase to a disordered phase in the second side. It seems that the energy dependence of both observables ($\langle R_{cent} \rangle$ and Δ-scaling) reflects the same fundamental mechanism. As suggested in Ref. 6 it could be related to the disappearance of heavy residues in central collisions. To conclude, the variety of observables showing contemporary signals of both dynamical and thermodynamical nature is very challenging for the microscopic transport models.

4. Heaviest fragment in peripheral collisions

An important question in the fragmentation regime concerns the physical quantity that drives the process. Indeed, an abundant literature exists on that subject (see for example [7–10]) and from the experimental works it is reasonable to admit various scenarios, involving different driving quantities. Here, we discuss the role of the excitation energy on the fragmentation and its correlation to the distribution of the heaviest fragment. For the analysis we use data from peripheral collisions measured for symmetric system with INDRA. The peripheral collisions are chosen since the same reaction provides a large range of dissipation. It is well known that peripheral collisions leads to a highly fragmented system with an abundant

materiel emitted in velocity range between target and projectile remnants and many mechanisms have been recognised like neck breaking, mid-rapidity emission or hierarchical rupture ([11–17]). In this analysis, we consider all the material emitted in the forward hemisphere of the c.o.m. The multiplicity M_{imf} of fragments Z$\geq$3 is deduced using event by event analysis techniques. The dissipated energy is defined as the excitation energy of a pseudo-source constructed with the M_{imf} fragments:

i) the pseudo-source velocity is deduced from the velocity of the M_{imf} fragments;

ii) the excitation E^* and size Z_{source} of the pseudo-source are estimated as in Ref. 18 (only light charged particles emitted in the forward hemisphere of the pseudo-source were considered and doubled).

An excitation energy E_{exc} is deduced event by event using a calorimetric method in the frame of the pseudo-source including all light charged particles. In both determination of the excitation energy, neutrons are estimated as in Ref. 18. A thorough data analysis has been performed to find out the pertinent correlations between the degree of fragmentation and the deposited energy. The striking features are presented in the following.

In Fig. 3 are reported the evolution of $\langle(M_{imf})/Z_{source}\rangle$ as a function of the excitation energy E_{exc}. The main feature is an increasing of the ratio with E_{exc}. A collapse is not observed. Fig. 4 shows the average value of $\langle(M_{imf}-1)/Z_{source}\rangle$ as a function of E^* for all studied systems. We observe that data fall down on a straight line except for a bending related to the tail of E^* distributions. It

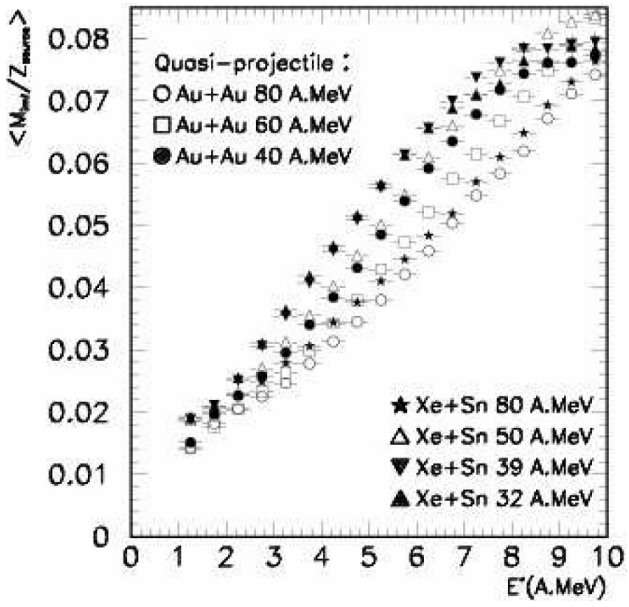

FIGURE 3. Evolution of the ratio $\langle(M_{imf})/Z_{source}\rangle$ as a function of the excitation energy E_{exc} for a quasi-projectile measured in Au+Au at 40-60-80 A MeV, Ta+Au at 40 A MeV, Ni+Ni at 32 A MeV and Xe+Sn at 25-32-39-45-50 A MeV.

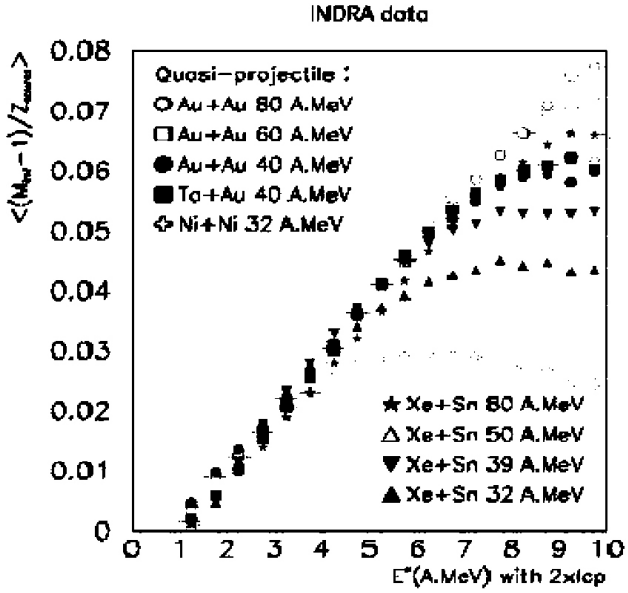

FIGURE 4. Evolution of $\langle(M_{imf}-1)/Z_{source}\rangle$ as a function of the excitation energy E^* for a QP measured in Au+Au at 40-60-80 A MeV, Ta+Au at 40 A MeV, Ni+Ni at 32 A MeV and Xe+Sn 25-32-39-45-50 A MeV.

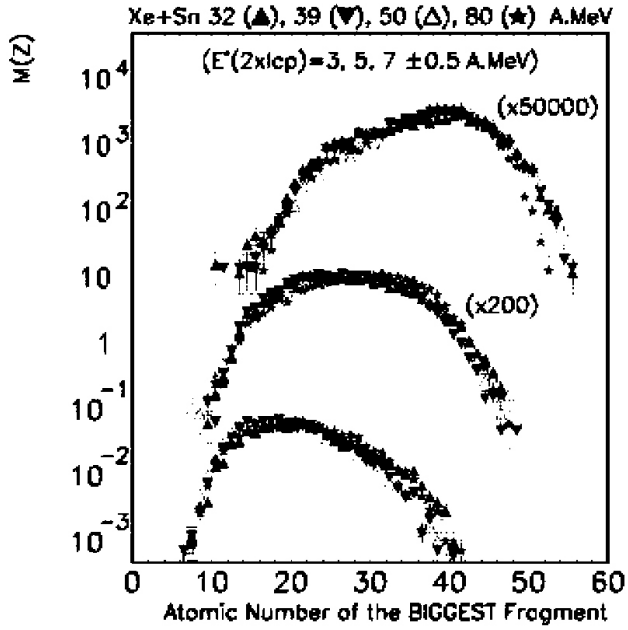

FIGURE 5. Size distribution of the heaviest fragment Z_{max} as a function of the excitation energy E^* (3, 5, 7 and A MeV) for a quasi-projectile in Xe+Sn 25-32-39-45-50 A MeV.

is worth noticing that other combination between various observables does not produce the scaling. Fig. 4 suggests to examine the size distribution of the heaviest fragment Z_{max} at the same E^* for different bombarding energy. This is shown on Fig. 5 for three ensembles at E^*=3,5 and 7 A MeV measured in the reactions Xe+Sn at 32, 39, 50 and 80 A MeV. First of all, at the same E^* the Z_{max} distribution scales perfectly. This is verified whatever the bombarding energy. It is also remarkable that the shape of the distribution changes

drastically from 3 to 7 A MeV and the scaling is still verified. It has been already observed that the distribution of the size of the heaviest fragment is governed by the excitation of the system as for example in the case of source formed in central collisions of Xe+Sn at 32 A MeV and Gd+U at 36 A MeV [19]. But in the present case, the independence is observed with respect to the bombarding energy. Concerning the size distributions of the remaining fragments measured in Xe+Sn from 32 A MeV up to 80 A MeV, the scaling is not observed globally, but below and above 39 A MeV indicating the presence of dynamical effects. For Au+Au the scaling is verified at E^*= 3 A MeV and becomes worst as bombarding energy increases. These could signal fragmentation processes of different origin or some influence of the size of the system.

5. Kinetic energy fluctuations

Modern studies on nuclear fragmentation have strongly contributed to the field of phase transitions in finite systems. Phase transitions are likely discussed in the context of macroscopic systems where transitions are observed through divergencies in quantities as the specific heat capacity. For systems as nuclei, those signatures are no longer valid. The adapted signatures to pin down phase transition in nuclei become anomalies in thermodynamical quantities, as for example a back bending in the caloric curve, abnormal fluctuations and negative heat capacity [20]. Besides to various signals as the caloric curve [21, 22] fingerprints of spinodal decomposition, [23, 24], scaling laws [6, 25–28], bimodality [29], the negative heat capacity [18] is actively searched for in data since such effects would indicate the occurrence of a phase transition. In this part we report on recent investigations on kinetic energy fluctuations (K.E.F) in quasi-projectiles (QP) formed at intermediate energies. As noticed in the previous section, it is well known that binary processes with a strong dynamical and neck component dominate symmetric nucleus-nucleus collisions. Here, a new method is proposed to filter the dynamical component in the fragmentation of a pseudo QP. Events are selected requiring that the total charge collected in the forward hemisphere of the c.o.m is representative of the incident projectile $\pm 10\%$. In this data set, the velocity of the source V_{source} is constructed with all fragments Z$\geq$3. The last step is to sum up all the projections of the fragment velocities onto the V_{source} direction and we call this variable V_{sel}. Two classes are clearly distinguished: collisions with a strong dynamical configuration are characterised by a negative value of V_{sel}, while neck or/and mid-rapidity emission are rejected when $V_{sel} \geq 0$. Extensive controls have shown that the selected variable is very efficient for excitation energy below 4 A MeV. The next step is to apply the procedure to measure the heat capacity for the selected sample.

For equilibrated nuclear systems the total excitation energy E* could be separated in two components $E^* = E_k + E_{pot}$ where E_k (E_{pot}) is the total kinetic energy (total configurational energy) respectively. The total heat capacity is defined as $c_{tot} = c_k^2/(c_k - A_0\sigma_k^2/T^2)$ where $c_k = dE_k/dT$ and the temperature T is estimated by solving the kinetic equation of state and A_0 is the size of the

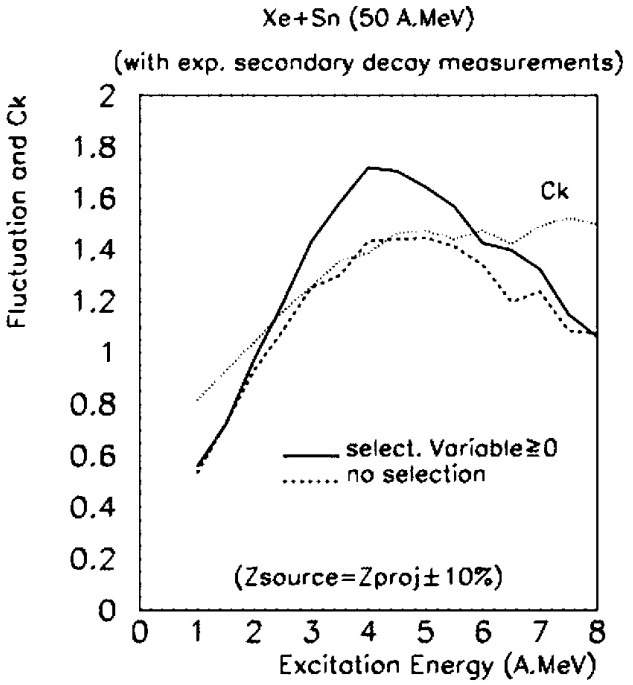

FIGURE 6. Kinetic heat capacity (dots) and normalized partial energy fluctuations with (line) and without (dashed line) selection with the variable V_{sel} for a quasi projectile in Xe+Sn at 50 A.MeV.

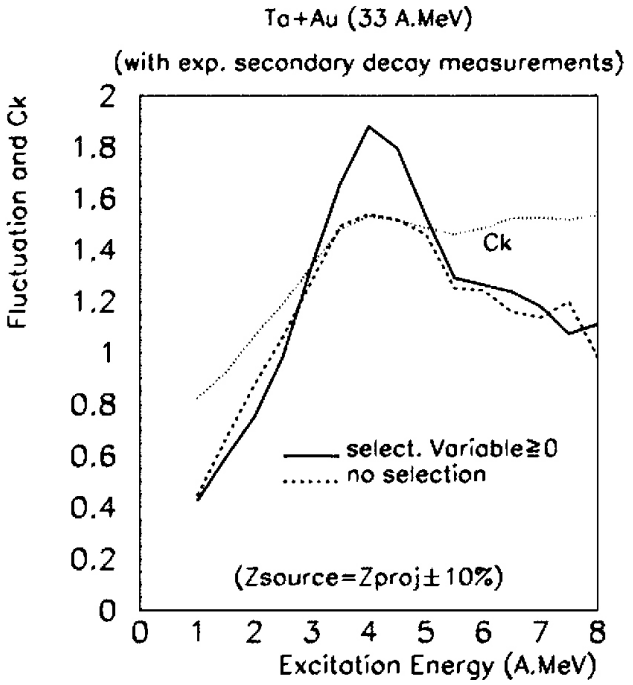

FIGURE 7. Kinetic heat capacity (dots) and normalized partial energy fluctuations with (line) and without (dashed line) selection with the variable V_{sel} for a quasi projectile in Ta+Au at 33 A.MeV.

source. In multifragmentation studies the total kinetic energy E_k should be determined at the freeze out stage, where partitions are no longer evolving and fragments are only interacting through coulomb potential. Such a configuration is not experimentally accessible but the heat capacity is extracted from the configurational energy (E_{pot}). The general procedure has been thoroughly checked [18].

Our results are presented in Fig. 6 (Fig. 7) for the Xe+Sn (Ta+Au) QP and Fig. 7 reactions. Data processing to get the relevant quantities is the same as the one presented in [18]. Normalized fluctuations $A_0\sigma_k^2/T^2$ calculated for Xe+Sn (full line in Fig. 6) shows a bell shape as a function of the excitation energy E^* with a maximum around 4 A MeV. c_k (dotted line in Fig. 6) increases with the excitation energy and crosses the normalized fluctuations at $E^* \simeq$2.5 A MeV and $E^* \simeq$5.5A MeV. Such crossings induce two divergencies and a domain where the total heat capacity becomes negative since $c_{tot} = c_k^2/(c_k - A_0\sigma_k^2/T^2)$. In Fig. 6 dashed line represent the result of the analysis when the variable V_{sel} is not used as event selector. In such case the magnitude of the maximal fluctuation decreases showing that the presence of dynamical process in the data sample tends to diminish the maximal fluctuation as demonstrated in recent theoretical work [20]. It is worth noticing that locations of crossing points and maximal value of normalized fluctuations are observed at same excitation energies in both INDRA and MULTICS-MINIBALL data [18]. Figure 7 shows the result of the analysis for Ta+ Au QP. Same conclusions as for Xe+Sn could be written.

Striking facts are also noticeable. In both reactions the four calculated K.E.F are bell shaped, and at high excitation energy the decreasing part of the kinetic energy fluctuations calculated by filtering with V_{sel} merge with the K.E.F obtained for the whole set of data. The maximum value of the new K.E.F exceeds clearly the canonical value and is smaller for the lighter system. Last, the peak of the new K.E.F seems weaker for the bigger system. All these features point to a size dependence effects, which require further investigations.

6. Summary

Fragmentation data are selected to discuss dynamical and thermodynamical features at intermediate energies. A wide systematic on nuclear stopping across the Fermi energy delineates the respective energy domain where mean field and nucleon-nucleon collisions dominate. A thorough study on quasi projectile shows a strong correlation between the excitation energy and the size of the biggest fragment even in the presence of a dynamical component. The lower branch of the negative heat capacity is observed around 3 A MeV for a quasi Xe and Ta projectiles. A large variety of observables have been discussed. It is really a challenge for the dynamical reaction models to be able to reproduce in the same framework such an ensemble of observables showing contemporary signals of both dynamical and thermodynamical nature.

1. J. Pouthas *et al.*, *Nucl. Instr. and Meth. A* **357** (1995) 418; J. Pouthas *et al.*, *Nucl. Instr. and Meth. A* **369** (1996) 222.
2. W.J. Llope *et al.*, (The NSCL 4π Group) *Phys. Rev. C* **52** (1995) 1900.
3. C. Escano-Rodriguez *et al.*, (INDRA Collaboration) nucl-ex (2005) 0503007.
4. A. Le Fèvre (INDRA-ALADIN Collaboration) *Nucl. Phys. A* **735** (2004) 219.
5. R. Botet and M. Ploszajczak, *Phys. Rev. E* **62** (2000) 1825.
6. J.D. Frankland *et al.*, (INDRA Collaboration) *Phys. Rev. C* **71** (2005) 034607.
7. L. Beaulieu *et al.*, *Phys. Rev. C* **64** (2001) 064604.
8. L. Beaulieu *et al.*, *Phys. Rev. C* **54** (1996) R973.
9. H. Hauger *et al.*, (EOS Collaboration) *Phys. Rev. C* **62** (2000) 024616.
10. P. Kreutz *et al.*, (ALADIN Collaboration) *Nucl. Phys. A* **556** (1993) 672.
11. C.P. Montoya *et al.*, *Phys. Rev. Lett.* **73** (1994) 3070.
12. J. Lukasik *et al.*, (INDRA and ALADIN Collaborations) *Phys. Lett. B* **566** (2003) 76.
13. Y. La Rochelle *et al.*, *Phys. Rev. C* **59** (1999) R565.
14. J.F. Dempsey *et al.*, *Phys. Rev. C* **54** (1996) 1710.
15. A. Pagano *et al.*, *Nucl. Phys. A* **734** (2004) 504c.
16. E. de Filipo *et al.*, (CHIMERA Collaboration), *Phys. Rev. C* **71** (2005) 064604.
17. J. Colin *et al.*, (INDRA Collaboration), *Phys. Rev. C* **67** (2003) 064603.
18. M. D'Agostino *et al.*, *Nucl. Phys. A* **650** (1999) 329; *Phys. Lett. B* **473** (2000) 219; *Nucl. Phys. A* **699** (2002) 795.
19. M.F. Rivet; (INDRA Collaboration) *Phys. Lett. B* **430** (1998) 217.
20. Ph. Chomaz *et al.*, *Phys. Rev. E* **64** (2001) 046114.
21. J. Pochodzalla *et al.*, (ALADIN Collaboration) *Phys. Rev. Lett.* **75** (1995) 1040.
22. J.B Natowitz *et al.*, (NIMROD Collaboration) *Phys. Rev. C* **65** (2002) 034618.
23. J.D. Frankland *et al.*, (INDRA Collaboration) *Nucl. Phys. A* **689** (2001) 940.
24. B. Borderie *et al.*, (INDRA Collaboration) *Phys. Rev. Lett.* **86** (2001) 3252.
25. N. Le Neindre *et al.*, *Proceedings of the International Workshop on Multifragmentation and related topics, Catania, December 2005, to be published*.

26. J.B. Elliot *et al. Phys. Rev. Lett.* **88** (2002)

27. M.K. Berkenbusch, W. Bauer *et al.*, *Phys. Rev. Lett.* **88** (2002) 022701.

28. Y.G. Ma *et al.*, (NIMROD Collaboration) *Phys. Rev. C* **71** (2005) 054606.

29. E. Bonnet, thesis in preparation, and *Proceedings of the International Workshop on Multifragmentation and related topics, Catania, December 2005, to be published*; B. Tamain *et al.*, same proceedings; O. Lopez *et al.*, same proceedings.

30. N. Le Neindre *et al.*, XL Int. Winter Meeting Bormio 2002, p. 144.